Reaction Chemistry & Engineering

ROYAL SOCIETY OF CHEMISTRY

PAPER

View Article Online
View Journal

Check for updates

Cite this: DOI: 10.1039/d3re00036b

Thermo-oxidative conversion of PDC as a molecular model of residual feedstocks to oxygen-rich chemicals†

Redhwan Al-Akbari,[a] Maryam Razi,[a] Ismail Badran[b] and Nashaat N. Nassar*[a]

Received 16th January 2023,
Accepted 6th February 2023

DOI: 10.1039/d3re00036b

rsc.li/reaction-engineering

Increased global energy consumption has resulted in more waste and greenhouse gas emissions. To reduce emissions, new technologies for treating and converting such waste with minimal CO_2 emissions are required. In this study, we investigated the thermal oxidative conversion of PDC, a model molecule for residual feedstocks, such as petroleum coke and asphaltenes, to value-added oxygenated chemicals. The investigation was performed experimentally and theoretically. Based on the experimental results, a lumped kinetic model was developed to determine the activation energies and rate constants of the reaction. The reaction route to form CO_2 was not preferred at the temperatures and pressures used in the reactions, as supported by TOC, FTIR, and GC-MS results. Furthermore, according to DFT calculations, –OH plays the most important role in the conversion of PDC, which results in the formation of more stable oxygenated intermediates.

1. Introduction

The global increase in energy demand results in massive CO_2 emissions. It is estimated that 34 gigatons of CO_2 are released into the atmosphere from the ongoing utilization of fossil energy resources.[1] The fossil energy industry also produces large quantities of waste. Examples of this waste include petroleum coke (petcoke) and asphaltenes, which are typically referred to as residual feedstocks. Petcoke is a highly dense heteroatomic hydrocarbon that is rich with sulfur, nitrogen, and oxygen atoms, in addition to heavy metals such as nickel, iron, and vanadium.[2] Petcoke is typically generated from bitumen and heavy oil upgrading processes. The global petcoke production is estimated to be 150 million tons per year, with North America accounting for 70% of the total.[3] Because of its limited market, petcoke is piled in refineries, causing an environmental crisis. Approximately, two-thirds of the produced petcoke is stored in refineries worldwide. Petroleum waste, such as petcoke, is typically treated and upgraded thermally, either through pyrolysis or gasification. Aside from producing greenhouse gases (*e.g.*, CO_2 and SO_2), such processes are energy intensive and require high capital. Asphaltenes are another type of fossil fuel waste; they are the densest, mostly polar, and surface-active fraction of oil.[4,5] The presence of asphaltenes causes several problems for oil wells, starting from plugging rock pores, deposition within wells, as well as coke formation. A negative feature of asphaltenes is their ability to aggregate and thus increase the viscosity of crude oil.[4–6]

Petroleum waste such as petcoke, asphaltenes, and heavy feedstock, have large and complex chemical structures. Our research team has developed a method to convert this waste into value-added oxygenated chemicals by oxidizing it using an alkaline solution at low temperature and pressure.[2] Such combination of thermal cracking and oxidation reactions is typically complex and proceeds through multiple and convoluted steps. Typically, to better understand the mechanisms underlying the reactivity of petroleum wastes, researchers proposed molecular models that have similar characteristics but are less complex.[5,7,8] These models were used in either experimental or computational studies to uncover certain characteristics of residual feedstocks reactivity.[9–11] The choice of the model molecule depends on its chemical properties such as the type of atoms involved, functional groups, and aromaticity, as well as physical factors such as porosity and particle size.

In the past couple of decades, several molecular models have been suggested to represent various residual feedstocks. These models served to capture various chemical and physical properties. With the advancement of computational

[a] Department of Chemical and Petroleum Engineering, University of Calgary, 2500 University Drive Northwest, Calgary, Alberta T2N 1N4, Canada.
E-mail: nassar@ucalgary.ca
[b] Department of Chemistry, Faculty of Sciences, An-Najah National University, Nablus, Palestine

† Electronic supplementary information (ESI) available. See DOI: https://doi.org/10.1039/d3re00036b

modeling, these molecular models became more complex, incorporating physical structure such as scale, aromaticity, atom heterogeneity, porosity, and orientation. For example, Manasrah *et al.* investigated the oxycracking of quinolin-65 as a model molecule for residual feedstocks to better understand the reaction mechanism.[5] Mullins *et al.* have introduced a modified Yen model for asphaltenes to account for the massive information discovered after the original proposal.[12,13]

In this study, we are proposing a new molecular model, *N*, *N*′-dipentyl-3,4,9,10-perylenedicarboximide (PDC, Fig. 1) to mimic thermo-oxidative behavior of residual feedstocks in an alkaline medium. This molecular model was chosen because of its similarity to the aromatic structure of residual feedstocks suggested by several studies.[14–18] PDC is a fused aromatic hydrocarbon, which contains heteroatoms such as nitrogen, and long alkyl side chains. It is an aromatic molecule that has not been fully oxidized (there are no OH or COOH groups). What is more, it is commercially available.

Studies showed that residual feedstocks, such as petcoke, undergo several bond-making and bond-breaking reactions when subjected to various ranges of temperatures and pressures.[3,19,20] Understanding how residual feedstocks react in an alkaline medium under different conditions is critical for unlocking the development of sustainable technologies that enable the production of value-added products. In turn, this will reduce the negative effects of thermo-oxidative reactions on the residual feedstock structure, such as CO_2 emissions. These simultaneous thermal cracking and oxidative reactions, known as oxycracking, have been successfully applied to multiple types of residual feedstocks such as asphaltenes, petroleum coke, and oil sands tailings.[3,6] In all cases, the conversion of solid hydrocarbons into oxygen-containing compounds is possible, with minimum to zero CO_2 formation. As a result, and in continuation of our previous work, this study investigates the application of oxycracking reaction on residual feedstocks molecular model (PDC) to gain a better understanding of how the reaction works and what steps are involved. This would help to unravel the complexities of residual feedstock structure and structure-behavior relationships in oxycracking.

The strength of the study relies on the combination of experimental work and theoretical computational calculations. Our aim from the oxycracking of residual feedstocks, represented by the PDC, is to produce high content of oxygenated products of high market value that can be used in industrial and agricultural applications. In this study, the oxycracking reactions were conducted under a high pressure of O_2 (5171 kPa) and an alkaline medium. Under these conditions, O_2 can be incorporated into PDC to form mildly oxidized intermediates and PDC can be functionalized with more OH and COOH groups. Thus, avoiding the complete oxidation of the molecule into CO_2 and H_2O. The basic medium (KOH) also helps the solubilization of the organic molecule since PDC is insoluble in water. KOH also helps in stabilizing the acidic products formed upon the reaction, which also minimizes the corrosion of reactor parts. The reaction products are characterized by different techniques, including TOC, FTIR, and GC-MS. A triangular lumped kinetic model is then implemented to determine the kinetic parameters of the reaction.

In our previous works on the oxycracking of organic molecules, including quinoline-65 and metformin, we studied the role of different oxidizing species such as O_2, $O^{\bullet}$, and $OH^{\bullet}$ on the oxycracking reactions.[5] It was long hypothesized that $OH^{\bullet}$ nucleophilic attacks on aromatic molecules are one of the most favorable pathways initiating their oxidation.[22–24] As the oxycracking of the model molecule (PDC) is taking place in the basic medium, we implemented density functional theory (DFT) calculations to study the reactions of PDC with hydroxide ion (OH^-); which happens also to be the solubilized form of $^{\bullet}OH$, to construct a reaction mechanism for the oxycracking.

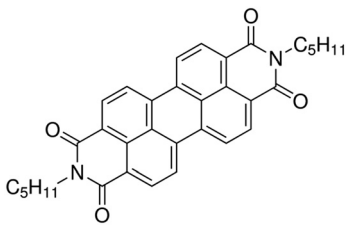

Fig. 1 Chemical structure of the model molecule, *N*,*N*′-dipentyl-3,4,9,10-perylenedicarbamide (PDC).

2. Experimental work

2.1 Materials

N,*N*′-Dipentyl-3,4,9,10-perylenedicarboximide (PDC, 98%) was purchased from Sigma-Aldrich (Ontario, Canada). The compound comes as powder and has a pinkish color. PDC has a chemical formula is $C_{34}H_{30}N_2O_4$ with a molecular weight of 530.61 g mol^{-1}. Potassium hydroxide (KOH) with purity of ≥85% in pellet form was purchased from Sigma-Aldrich (Ontario, Canada) and used as alkaline source. Oxygen with a purity of 99.9% was purchased from Praxair (Calgary, Canada) and used as oxidizing agent. All the chemicals were used as received without further purification.

2.2 Experimental apparatus, procedures, and conditions

PDC was added to a mixture of KOH and deionized water. Most experiments were run at a ratio of 1 : 1 KOH to PDC. Amounts of PDC used were from 25–50 mg in 15 mL of water. Once the three major components were mixed, oxygen was introduced into the reactor from a cylinder. The oxygen pressure was maintained at 5171 kPa. The reactor used is 100 mL Parr reactor with model number 4598 purchased from Parr Instrument Company, Moline, IL, USA. The reactor vessel is equipped with a furnace to supply heat to the reactor. The temperature of the furnace and the solution inside of the reactor are controlled using a PID controller in the control panel. Pressure and mixing speeds are also

controlled using the control panel. The mixing speed in our experiments was fixed at 1000 rpm for all experiments as this has been proven to be the optimal mixing speed to avoid any mass transfer limitation and avoid any variation in concentration and temperatures in the whole reactor volume. Three temperatures were examined for the oxycracking of PDC namely 150, 200 and 230 °C, and pressure was fixed at 5171 kPa as proven to be the optimal pressure from previous work.[3] Once all materials are in the reactor and pressure is achieved, the temperatures are then set to the desired ones. The zero time of the reaction was considered when the temperature of the reactor reaches the desired value. The times chosen are 0.5, 1, 1.5 and 2 h. Once the reaction is finished, the reactor is left to cool down to room temperature before the content of the reactor is removed. The liquid portion of the reactor content is collected, and the reactor is then washed with deionized water to recover any insoluble PDC. The liquid portion is centrifuged to force the suspended particles to settle. The solid was collected to measure the residue content. Liquid and solid portions were characterized using TOC, FTIR, GC/MS, and CHNS to get deep understanding about the virgin PDC, oxycracked products and the residues. A sample of the gas was collected to measure the amount CO_2 in the gas phase. Fig. 2 (also Fig. S1†) shows a simplified schematic of the experimental setup with the reactor, control panel that receive three signals (pressure, temperature, and rpm), an oxygen tank and some of the steps used after collecting the products.

2.3 Fourier transform infrared spectroscopy (FTIR)

A Fourier transform infrared spectrophotometer (IRAffinity-1S, Shimadzu Corporation, model no. 3116465 Mandel, USA) was used to get the IR spectra for PDC, solubilized PDC and residual PDC. FTIR allows for the identification of chemical substances and functional ground based on the adsorption frequency. All samples were dried in a vacuum oven at 62 ± 3 °C before using them in FTIR analysis. The samples were all mixed with KBr, which is used as a reference for the spectra. The number of scans was chosen to be 50 and the scan range was taken between 400 and 4000 cm^{-1}.

2.4 Total organic carbon (TOC)

Shimadzu Total Organic Carbon Analyzer (TOC-L CPH/CPN, Mandel, USA) was utilized to measure the total organic carbon (TOC), inorganic carbon (IC) and total carbon (TC). The TOC analyzer has three stages starting with acidification going through oxidation and ending with detection and quantification. Acidification causes the liberation of carbonates and bicarbonates to CO_2. The remaining carbon is then converted to CO_2 with high-temperature catalytic oxidation. 1 mL of the centrifuged liquid portion was diluted with 12 mL of deionized water. After dilution, the mixtures were sonicated to homogenize the solutions. The TOC vials are transferred to the device and TC, TOC and IC are measured. The device takes three injections from each sample to prove reproducibility. The TOC measurement is important since it gives us an idea of how much PDC was solubilized in the liquid in terms of carbon. And these measurements were later used in the mass balance for carbon to carry out the kinetics calculations.

2.5 Elemental analysis (CHNS analysis)

The device used to measure the carbon, nitrogen and hydrogen content is PerkinElmer 2400 Series II (Waltham,

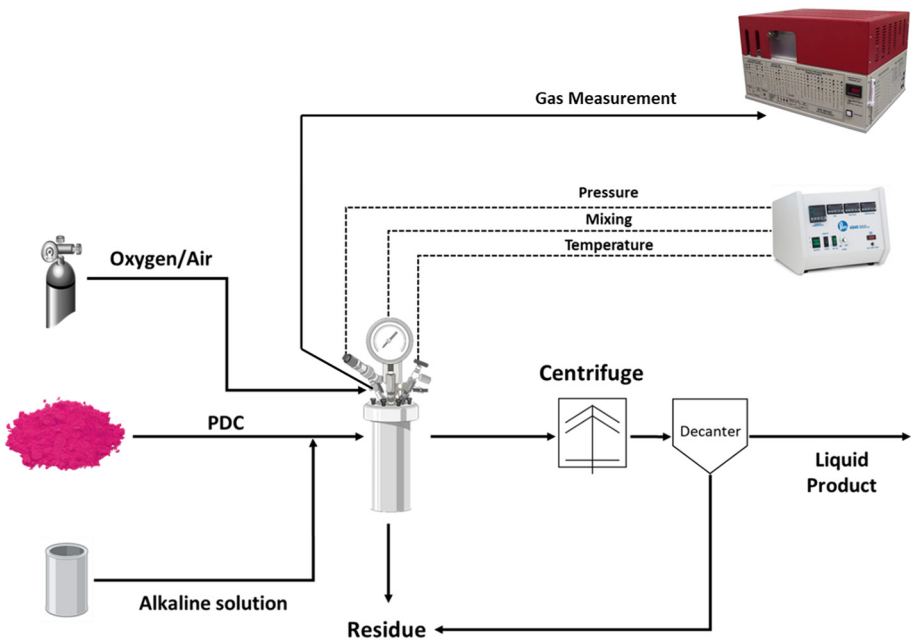

Fig. 2 Simplified experimental setup showing the Parr reactor, signal monitoring system and the oxygen supply.

Massachusetts, USA). The device operates by flash combustion method where the gases resulting from the combustion are analyzed using thermal conductivity detector. The device was used to measure the CHNS content in the virgin material, oxycracked material, and residues after the reaction. All samples were dried and homogenized, and the analysis was repeated three times to ensure reproducibility. The results used to verify the theoretical formula of *N*,*N*′-dipentyl-3,4,9,10-perylenedicarboximide and the carbon content used to construct a mass balance to make sure all products are accounted for in the reaction. Then, once the mass balance was verified, the lumped reaction kinetic model was constructed based on carbon. Oxygen content was taken as the difference between the sum of C, N, and H and 100. The oxygen content allows for the verification of the oxygen incorporation in the oxycracked PDC.

2.6 GC-MS analysis

Selected sample of the liquid phase of the reaction mixture was analyzed by gas chromatography-mass spectrometry, GC-MS (Agilent 6890, USA) equipped with a mass selective detector system (Agilent 5975 MSD, USA). The components were separated through a mid-polar column (50% polar) (Agilent, DB17ms, USA). In a typical analysis, 2.0 microliter of 1% diluted sample in methanol was injected at 250 °C into the GC-MS. Oven temperature was held constant at 40 °C for 2 min and ramped at 10 °C min^{-1} to 280 °C. The temperature was then held at 280 °C for 8 min. Helium (28.5 kPa) was used as a carrier gas at a flow rate of 1.0 mL min^{-1} in splitless mode. The analysis was performed in electron ionization (EI) positive ion mode in the scan range 35–700 *m*/*z*, scan interval = 0.56 s, and scan speed = 1562 unit per s. The NIST mass spectral library 2020 was used to analyze the reaction products.

2.7 Reaction kinetics calculations

The experimental data collected from multiple experiments conducted at three different temperatures and times, was used to perform a mass balance on carbon and calculate the conversion and yield. The amount of carbon in feedstock was obtained theoretically and compared to the experimental results found from elemental (C,N,H,S) analysis. The products and residues were then collected and analyzed using TOC and elemental analysis to obtain their carbon content. The mass balance results in 94% to 97% accuracy. Once the mass balance was obtained, the kinetics calculations were carried out using rate laws and Arrhenius equation. The lumped kinetics triangular method was constructed for the reaction.[25] The feedstock (PDC) is either converted to intermediates or CO_2. Intermediates also can be converted to CO_2 under further cracking and oxidation. To minimize that, KOH was used to solubilize the intermediate in the solution and prevent further reaction to CO_2. More about the calculations, mechanism and kinetics will be discussed in the results section of this paper.

2.8 Theoretical calculations

The reactions of the PDC model molecule with ^{-}OH were explored by DFT quantum calculations using Gaussian 16.[26] Full geometry optimization followed by frequency calculations for all species were performed using the M062X Minnesota functional along with the 6-31+G (d, p) basis set.[27] This method has demonstrated good performance in describing molecular geometries and energy predictions for similar systems.[28,29] The transitions states (TS) described herein were discovered by exploring the potential energy surface (PES) along the reaction coordinate of interest. For each TS, a single imaginary frequency was confirmed along the desired reaction coordinate and further validated by intrinsic reaction coordinates (IRC). As suggested by Scott and Radom, zero-point energies (ZPE) were scaled by a factor of 0.9631.[30] Since the oxycracking reactions take place in an aqueous media, explicit solvation was used by including the scrf = (solvent = water) and the empirical dispersion = GD3 keywords as required by the M062X functional. Further details on the energy calculations can be found elsewhere.[25,29,37]

3. Results and discussion

3.1 Reaction kinetics evaluation

The oxycracking reaction of PDC was studied experimentally under various temperatures and reaction times. There can be multiple parameters that play a factor in the reaction such as the reactor impeller speed and oxygen partial pressure, but these parameters have been fixed in this study. The impeller speed was fixed at around 1000 rpm for all experiments, as previous studies on oxycracking and wet air oxidation showed an acceptable range 500 and 1500 rpm, and the reaction rate was shown to be independent of impeller speed.[3,5,21,31,32] We chose to supply excess oxygen to avoid having the reaction limited by oxygen partial pressure. It is also important that water remains in the liquid phase throughout the reaction. For that to occur, the pressure must be higher

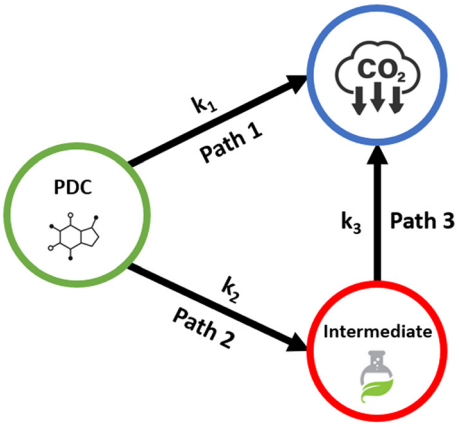

Fig. 3 Triangular lumped reaction kinetics model for the oxycracking of PDC.

than the vapor pressure of water at the desired temperature.[33–37] The partial pressure of oxygen was fixed at 5171 kPa initial pressure as higher pressures did not achieve better conversion based on other studies.[3]

In this study, we are proposing the triangular lumped kinetics model shown in Fig. 3. The model proposes that PDC is thermally cracked and partially oxidized into intermediates, which in turn decompose into CO_2 and water, depending on the severity of the reaction. On the other hand, PDC itself can decompose directly into CO_2 and H_2O. The triangular model has been adopted by many researchers for oxycracking and wet air oxidation of organics and residual feedstocks including petroleum coke, asphaltenes, coals, phenols and water organic pollutants.[3,21,31,38] It is, therefore, important to optimize the reaction conditions to arrive at more intermediates (favoring pathway 2) and prevent further oxidation into CO_2 and water. The intermediates represent the desired products, as in the case for residual feedstocks, these intermediates can be valuable solubilized acids such as humic and fulvic acids analogs. These intermediates have been observed in the FTIR analysis as will be explained in the following sections. Our DFT calculations have proven this and showed that lowest energy pathway would result in oxygenated compounds. KOH was added into the reaction to allow the intermediate compounds to be solubilized in water as salts. This has proven to reduce the further oxidation of these compounds and help with the stabilization of the intermediates. KOH optimization has been carried out in previous studies to arrive at the optimal dosage needed for the reaction.[3,5] It was found that 1 : 1 ratio of KOH to feedstock is ideal to achieve the desired results, as higher concentration of KOH is not needed.

To carry out the calculations for the kinetics of the reaction, a mass balance on carbon has been obtained based on the following equation:

$$m_{A_0} = m_L + m_g + m_R \tag{1}$$

where m_{A_0} is the carbon content in the original PDC, m_L is the carbon content in the liquid phase, m_g is the carbon content in the gas phase and m_R is the carbon content in the residual solids. m_{A_0} was obtained by multiplying the mass of PDC used in the reaction by the percentage of carbon found using CHNS analysis. The liquid portion (m_L) was taken from the TC measurement obtained from the TOC analyzer. The residue (insolubilized PDC) collected after the reaction, was analyzed using CHNS elemental analysis to find the percentage of carbon and was taken as m_R. m_g was obtained from correlations performed using previous studies on different materials. Once the mass balance was closed at 94% to 96%, the concentrations of the three species involved in the triangular model were calculated based on the experimental data (C_A, C_B, C_C). C_A represents the concentration of PDC throughout the reaction, which means that this concentration is decreasing with time. C_B shows the concentration of the intermediates or solubilized materials, and it is one of the products for that reason it is expected to increase with time. C_C is the concentration of CO_2. The concentration of PDC was calculated based on the conversion from the following equation

$$C_A = C_{A_0}(1 - X) \tag{2}$$

where X is the conversion. Once the concentrations of all species were calculated, the power rate law that relates concentration to time through ordinary differential equations was used. Since there are three pathways in the lumped kinetic model then there will be three ordinary differential equations to solve simultaneously for each temperature with initial conditions: $C_A\ (t = 0) = C_{A_0}$ and $C_B\ (t = 0) = C_C\ (t = 0) = 0$. To simplify the solution, the orders of the reaction were assumed first (n_1, n_2) at different combinations. The ones chosen at the end were the ones that resulted in the lowest error upon solving fitting the ODEs with the experimental data. The following are the ODEs that were solved to get rate constants.

$$\frac{dC_A}{dt} = -r_A = k_1 C_A^{n_1} + k_2 C_A^{n_1} \tag{3}$$

$$\frac{dC_B}{dt} = r_B = k_2 C_A^{n_1} - k_3 C_B^{n_2} \tag{4}$$

$$\frac{dC_C}{dt} = r_C = k_1 C_A^{n_1} + k_3 C_B^{n_2} \tag{5}$$

MATLAB R2021a was utilized to solve the differential equations using the ode45 function.[39] The rate constants (k_1, k_2 and k_3) were obtained at three different temperatures. These values are then used to graphically solve the Arrhenius equation to find the apparent activation energy (E_i) and the pre-exponential factor (A_i) according to the following equation.

$$k_i = A_i e^{\frac{-E_i}{RT}} \text{ or } \ln(k_i) = \ln(A_i) - \frac{E_i}{RT} \tag{6}$$

Fig. 4 shows the concentration profiles for the three species used in the model. The concentration profiles were obtained at three temperatures 230, 200 and 150 °C. As seen, as time increases PDC concentration (C_A) decreased and converted into intermediates (C_B) and CO_2 (C_C). However, it is clear, that the level of conversion is favored towards the intermediates rather than CO_2. When comparing the data at various temperatures, one can see that temperature is also an important factor. As the temperature increases, the rate of reaction (slope of the red curve) is higher. This means more products, specifically, more intermediates. It has been well established that the wet oxidation of organic materials is well described as first-order reaction and this is what we have obtained in this study, since PDC resembles the residual feedstocks, it should behave the same.[25,40,41] The formation of oxygenated intermediates and CO_2 in this study agrees well with studies performed on asphaltenes, petroleum coke and organic materials.[25,32,41] The existence of oxygenated

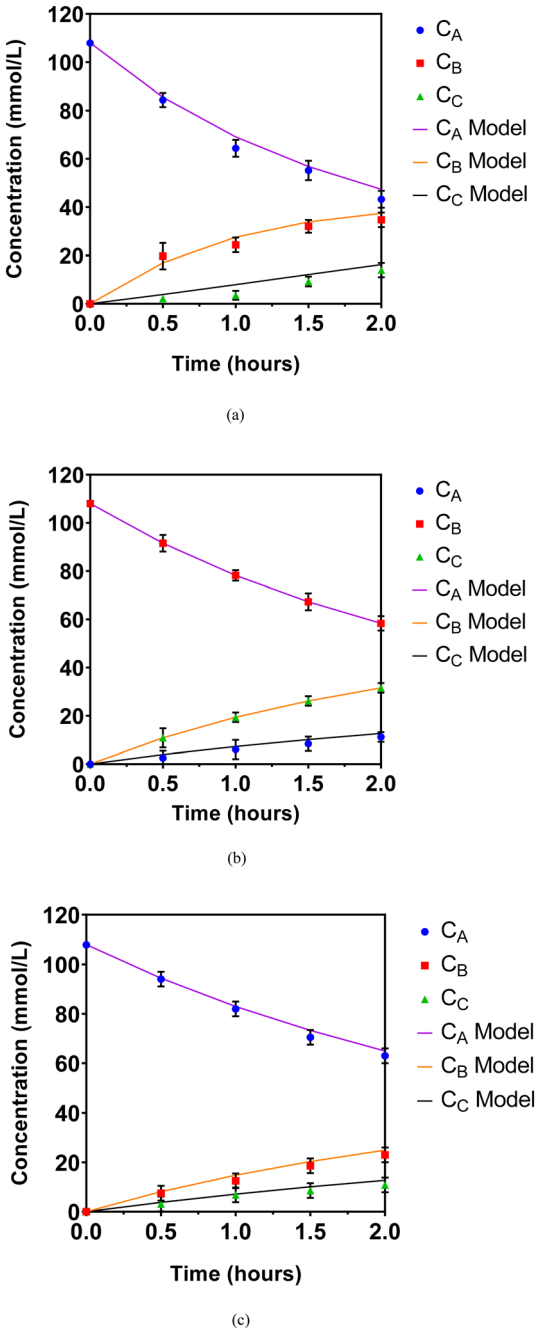

Fig. 4 Concentration profiles for PDC, intermediates (oxycracked PDC), and CO_2 at (a) 230, (b) 200, and (c) 150 °C, respectively at 5171 kPa with an impeller speed of 1000 rpm and 1:1 ratio of virgin PDC to KOH. Solid lines represent modeling data while points represent experimental data. Error bars represent the standard deviation of three replicates.

intermediates has been verified using TOC, FTIR and GC-MS analysis.

Table 1 shows the rate constants obtained from solving the previous ordinary differential equations at three temperatures. Rate constants are highest at 230 °C, since at higher temperatures the molecules have higher energy to overcome the activation energy barrier and PDC is oxycracked. Another observation is the lower rate constants at the third pathway in the lumped kinetic model. This gives an indication that the intermediates (oxycracked PDC) formed in the liquid are so stable. This can be due to the addition of KOH into the water that causes the oxygenated compounds to be converted in salts and that prevents further oxidation to CO_2.[41,42] Comparing the rate constants at pathways 1 and 2, we see that pathway 1 has lower rate constants at all temperatures than pathway 2, indicating the reaction is favoring the intermediates formation, rather than the full oxidation to CO_2 and H_2O.

Table 1 Reaction rate constants, determined experimentally by solving the concentration profiles, ordinary differential equations (ODE)s, obtained at three temperatures

T (°C)	150	200	230
k_1	0.015	0.052	0.108
k_2	0.035	0.092	0.16
k_3	8.79×10^{-5}	9.15×10^{-4}	1.61×10^{-3}

Table 2 shows the apparent activation energies and pre-exponential factors obtained graphically by solving the Arrhenius equation (Fig. 5). Pathway 1 that represents the complete oxidation of PDC to CO_2 and H_2O has an activation energy of 42.2 kJ mol^{-1}. This activation energy is lower than those reported for residual feedstock oxidations.[3,20,43] The highest activation energy was calculated for pathway 3, where the intermediates are further converted into CO_2 and H_2O. This is expected as the oxygenated compounds are more stable in the water and the energy barrier to convert them to CO_2 is higher. The lowest activation energy was found for pathway 2, where PDC is being transformed into solubilized oxygenated compounds. This value is close to what was obtained in DFT calculations in this study.

It is worth noting that the values obtained in this study are low compared to previous studies. This can be attributed to the smaller and less complex structure of PDC compared to the real structure of residual feedstocks.

3.2 FTIR analysis for virgin, oxycracked and residual of PDC

Fig. 6 shows the FTIR spectra for the virgin PDC, the oxycracked PDC, and its residue at 230 °C reaction temperature and 1 h reaction time. The IR spectrum of the virgin PDC shows sharp peaks around 2750–3000 cm^{-1}, which are associated with symmetric and asymmetric aliphatic C–H stretching. This is most likely attributed to the

Table 2 Reaction activation energies and pre-exponential factors for the three pathways proposed in the lumped kinetic model presented in Fig. 3

Activation energy (kJ mol^{-1})		Frequency factor (s^{-1})	
E_{a1}	42.2	A_1	2.50×10^3
E_{a2}	33.9	A_2	5.33×10^2
E_{a3}	66.3	A_3	1.46×10^3

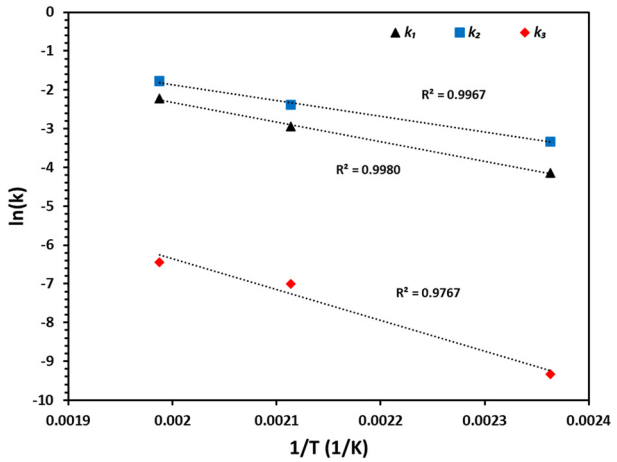

Fig. 5 Arrhenius plot for the determined values for rate constants plotted against reciprocal of temperature.

aliphatic side chain in PDC. It is noticed that the peaks in this region did not significantly change upon the oxycracking of the molecule. This infers that the OH^- attacks on the molecule did not proceed through the aliphatic chain but rather on the aromatic part. DFT calculations are in great agreement with this conclusion obtained through experimental findings as will be discussed later. Three strong peaks also appear between 3250 and 3500 cm^{-1} in the virgin PDC spectrum. These correspond to aromatic C–H stretching, as confirmed by DFT frequency calculations. The intensity of these peaks became much weaker in the oxycracked PDC, while they mostly retained in the residue. While this could be explained by the replacement of hydrogen atom in the aromatic part of the molecule by other functional groups, the weakening of the peaks might also be caused by the overlap with a broad peak in the same region due to O–H stretching. There is also a broad peak appearing after oxycracking in the 2600–3200 cm^{-1} region, which is attributed to the O–H stretching in carboxylic acids. Organic acids exhibit string IR absorption at around 1700 cm^{-1}. But PDC has already two carbonyl groups in its structure (*ca.* Fig. 1), so the appearance of 1700 cm^{-1} peak might refer either to ketone or acid. Nevertheless, the broad peak in the 2600–3200 cm^{-1} is good evidence for the formation of acids upon oxycracking. Overall, the FTIR results confirm the formation of oxygenated functional groups in the oxycracked PDC that did not appear in the virgin PDC. Which in turn, with TOC and GC/MS analysis, confirm the formation of intermediates that resembles organic acids produced during the oxidation of residual feedstocks.

3.3 Elemental analysis for virgin, oxycracked and residual PDC

Fig. 7 shows selected samples from the CHN analysis for virgin PDC, along with the oxycracked products obtained in the liquid after the reaction at three reaction temperatures, and the insoluble residual left after the reaction. Since the formula for PDC is known, the only element not accounted for in the analysis is oxygen, therefore, it was taken as the difference of 100% minus the sum of all elements. As seen, there is a difference between the virgin PDC and the oxycracked one, and the amount of carbon in the oxycracked PDC is significantly lower than in the original. This is a clear indication of oxygen incorporated into the sample. This incorporation can be in the form of carboxylic and phenolic type as has been shown in the computational modeling and GC-MS. This also agrees well with the results found from the FTIR and TOC analysis. However, looking at the residue after the reaction, we can conclude that it is not a different material but rather it is the same as the virgin PDC as also has been seen in the FTIR spectra. The elemental analysis also shows the temperature has no effect on the residue quality but rather quantity. Higher temperatures favor higher conversion of PDC, and lower residue left over but does not change the residue structure. This also proves the validity of the kinetics calculations since the residue was considered as

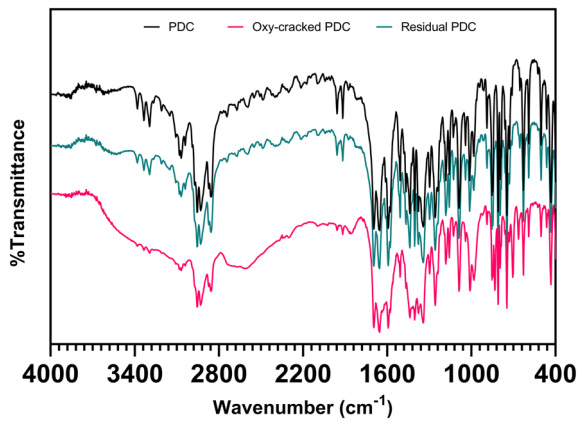

Fig. 6 FTIR spectra of virgin PDC and oxycracked PDC at 230 °C and 1 h reaction time, and the residual formed during the same reaction operating conditions.

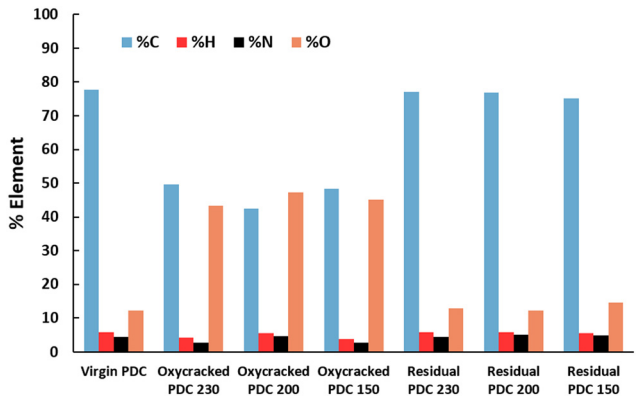

Fig. 7 Elemental analysis for virgin PDC, oxycracked PDC and residual PDC at three temperatures (230, 200, 150 °C), time of the reaction was 1.5 h.

unreacted PDC and not a by-product. It is also observed that the oxycracked PDC did not differ much in nature when temperature changed. This indicates that temperature does not affect the type of product generated but rather the quantity. Comparing the results obtained in this study to the literature, specifically in humic acids production from residual feedstocks and coals, there seems to be a clear agreement.[44–48] This gives us more confidence that PDC is a well-fitted model molecule to represent residual feedstocks as it shows similar behavior under thermo-oxidative environment.

3.4 GC-MS interpretation

The total ion chromatogram (TIC) for the oxycracked liquid phase of the model molecule PDC is shown in Fig. 8. The spectrum shows a strong peak around 26.5 min, along with other minor peaks at earlier retention times. A close analysis to the mass spectra obtained for the main peak is shown in Fig. S2 in the ESI.† PDC has a molecular weight of 530 g mol^{-1}, and the parent ion peak is clearly missing from the spectrum. This is not an uncommon observation for organic compounds that are analyzed by electron ionization.[49] We attempted to run the sample using soft ionization techniques to confirm the identity of this peak, but this was unsuccessful mostly due to the complex and heavy structure of PDC.

The mass spectrum in Fig. S2† shows a common ion series of 65, 77, 91, 105, and 117 *m*/*z*. Such a pattern indicates the presence of an aromatic structure with electron-donating substituents. The intense peak at 91 *m*/*z* is specific for benzyl group ($C_6H_5C^+H_2$) resulting from the photo degradation of the parent ion. There are other peaks at higher *m*/*z* of 194, 207, 253, and 312, which also could represent photo fragments of higher masses. This information suggests that the strong TIC peak in our chromatogram at 26.5 min is mostly due to the presence of PDC or a functionalized version of it in the reaction mixture. Fig. 8 also shows a small TIC peak at ~9 min which likely corresponds to an amine as suggested by the NIST mass spectral library. The mass spectrum of this peak is shown in Fig. S3† with a cluster of peaks maximized at 44 *m*/*z* and a missing parent ion peak. Such behavior is consistent with the mass pattern of primary and secondary amines. Among several suggested structures, *N*-methyl-1-pentanamine would be the most logical one to be formed upon the oxycracking of PDC. Such compound can be a product of C–N bond ruptures followed by ring-opening, as discussed later in the DFT calculation section.

Interestingly, the oxycracking of PDC did not produce many fragments as obtained by the GC-MS analysis. In our previous work on metformin, a nitrogen-rich small organic drug, its oxycracking under similar conditions managed to produce several transformation products including amines, amides, and urea derivatives.[21] PDC has mainly formed a single functionalized molecule, represented by the major peak in Fig. 8. This can be explained by the rigid aromatic structure of PDC that is difficult to degrade under our experimental conditions.

3.5 Oxycracking reaction mechanism by DFT calculations

Oxycracking of organic compounds can be initiated by different reactive species including O_2, O, and $^{\bullet}OH$. Several studies showed that $^{\bullet}OH$ and its solvated form ^{-}OH, play an important role in initiating the oxidation; especially in basic media. It is well known that $^{\bullet}OH$ nucleophilic attack on aromatic rings forms an Ar–$^{\bullet}$OH adduct followed by solvent dehydration into a phenoxyl radical R–O$^{\bullet}$.[24] Such dehydration is easily catalyzed by a base.

In our recent works, we showed that shortening the alkyl side chain does not largely affect the energies of the reactions, while it significantly speeds up the computational calculations.[5,21] Therefore, we reduced the alkyl chain in PDC down into two carbons, and the new structure is referred herein by PDC-s. Fig. 11 illustrates different attacks of ^{-}OH on PDC-s as explored under M062X/6-31+G(d,p) level of theory. In the first mechanism, ^{-}OH attacks C3, which is in the β position to the C═O group, forming the adduct M1. We have located the transition state for this reaction and an

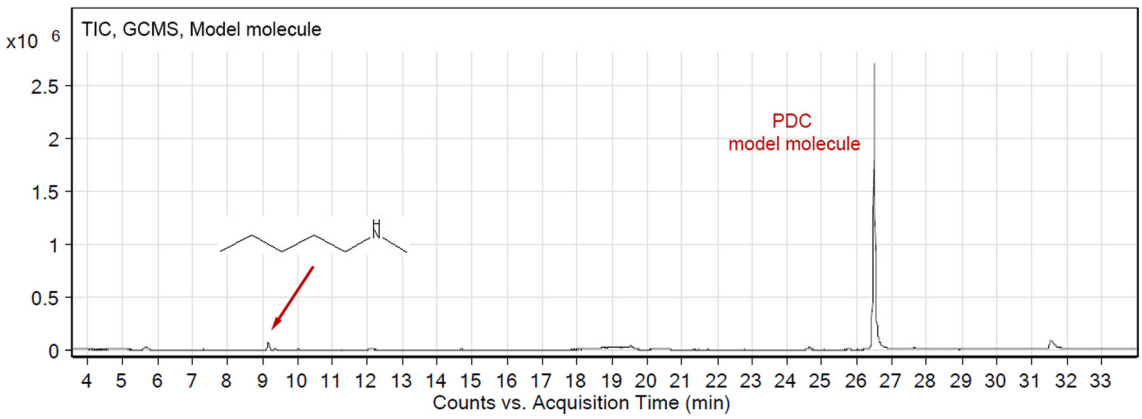

Fig. 8 Total ion chromatogram (TIC) for the oxycracked liquid phase of PDC obtained by GC-MS.

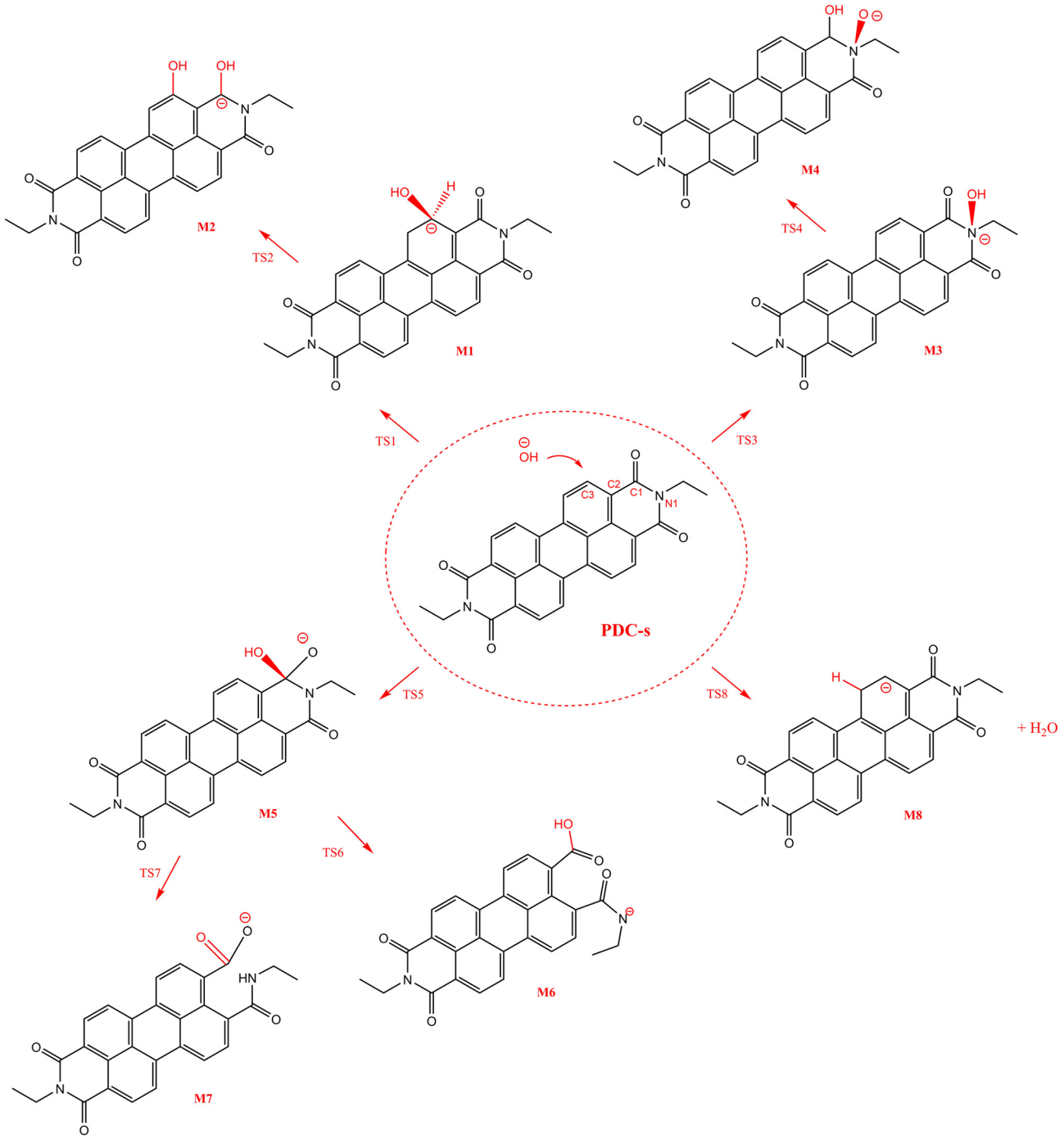

Fig. 9 Oxidation of PDC-s initiated by ⁻OH attacks as obtained at M062X/6-31+G (d,p) level of theory.

optimized geometry for TS1 is shown in Fig. S4.† The TS shows an imaginary frequency of 307.2i cm^{-1} corresponding to a strong HO···C3 stretching. An H-shift to the terminal oxygen is followed through TS2 forming the M2 intermediate, as shown in Fig. 11. Now M2 has two OH groups and its formation can be verified by the broad OH stretching peak detected by our FTIR, as discussed in section 2.3. The Gibbs free energy diagram for this mechanism is depicted in Fig. 10. The first barrier is computed at 58.6 kJ mol^{-1}, and M1 is more stable than the PDC-s/⁻OH system by about 23.4 kJ mol^{-1}. The barrier is close to what has been obtained for ⁻OH attacks on quinoline-65.[5] In a study by Kóňa *et al.*, the $\Delta G^{\ddagger}$ for the OH^- attack on a smaller aromatic molecule was 133 kJ mol^{-1} at B3LYP/6-31+G(d) level in aqueous solution.[23] Our computed barrier is much less than that value, which reflects the feasibility of this reaction in the case of PDC-s. As for the 2nd step in this mechanism, the $\Delta G^{\ddagger}$ for the H-shift through TS2 is high (167.8 kJ mol^{-1}), but the energies for M1 and M2 are close, with M2 being slightly more stable than M1.

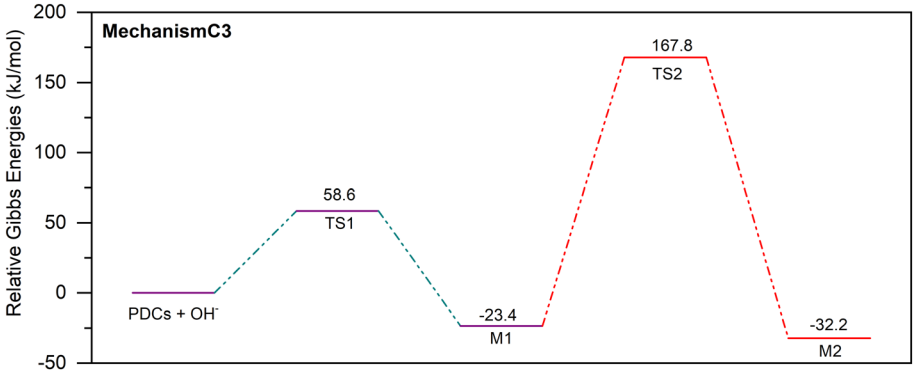

Fig. 10 Potential energy level diagram for ⁻OH attack on C3 in PDC-s. Energies represent relative Gibbs free energies in kJ mol^{-1} at 298 K and 1 atm (ZPE corrections are included).

Fig. 9 shows another possible ⁻OH attack on N1 in PDC-s. The transition state for this route is labeled TS3 and is shown in Fig. S5.† The imaginary frequency of this TS is 1406.3i cm^{-1} and it corresponds to a strong HO···N1 stretching. The activation barrier in terms of $\Delta G^{\ddagger}$ for this attack is 322 kJ mol^{-1}, as illustrated in Fig. 11. This is relatively a high barrier that makes such attack unfavorable. This is because of the difficulty of adding a negatively charged hydroxide ion to the electron-rich nitrogen center. The formation adduct M3 can proceed to form M4 through another transition state, TS4, as illustrated in Fig. 9. This transformation takes place by an H-shift to the O atom with a barrier of 274.1 kJ mol^{-1} with respect to the PDC-s/⁻OH system. This shift is much more favorable than that in the previous mechanism (C3) as it is 1,3-shift compared to a 1,4 shift in the C3 mechanism.

Another suggested reaction pathway is when ⁻OH attacks C1 in PDC-s. Such an attack can proceed through TS5, shown in Fig. S6,† with a single imaginary frequency of −220.7i cm^{-1}. The attack forms an addict, M5. The reaction proceeds through another transition state, TS6 which carries a single imaginary frequency of 134.2i cm^{-1}, corresponding to a C1–N1 bond stretch. This causes a ring opening to form the intermediate M6. Alternatively, an H-shift from oxygen to nitrogen in M5 can take place through TS7 to form the intermediate M7. The latter is another form of M6 once it is hydrated by a solvent, and it carries both a carboxylic acid and amid groups. The formation of these functional groups can be verified by the results of our FTIR and GC-MS analysis.

The potential energy diagram for the C1 mechanism is shown in Fig. 12. The first activation barrier in terms of the $\Delta G^{\ddagger}$ is only 41.0 kJ mol^{-1}. The formation of M5 is slightly exergonic with $\Delta_r G$ = −10.9 kJ mol^{-1}. This makes the attack on C1 the most favorable route in this study. Both TS6 and TS7 have also low barriers that are close to each other; but the formation of M7 is more thermodynamically stable, as its $\Delta_r G$ = −55.2 kJ mol^{-1}, where that of M6 is endergonic with $\Delta_r G$ = 36.0 kJ mol^{-1}.

It is worth mentioning that the attack on C1 is close to the ⁻OH attack on carbonyl in formamide (42.7 kJ mol^{-1}).[50] Also, it is close to what has been obtained for the same attack on a carbonyl at B3LYP/6-311++G (3df,pd) level of theory (49.8 kJ mol^{-1}).[51] Both values were obtained in solution.

The last reaction we considered is the H abstraction from PDC-s by ⁻OH. Fig. 9 illustrates that the hydroxide ion can abstract an aromatic hydrogen to form the intermediate M8. The transition state for this reaction was successfully located and was labeled TS8 (Fig. S7†). The imaginary frequency is

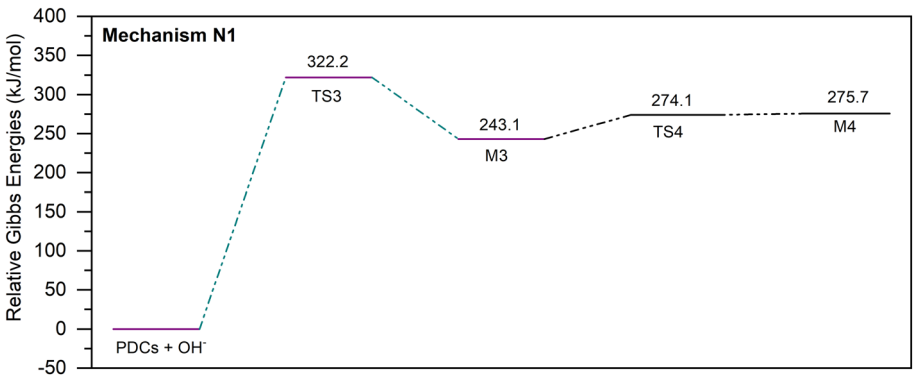

Fig. 11 Potential energy level diagram for ⁻OH attack on N1 in PDC-s. Energies represent relative Gibbs free energies in kJ mol^{-1} at 298 K and 1 atm (ZPE corrections are included).

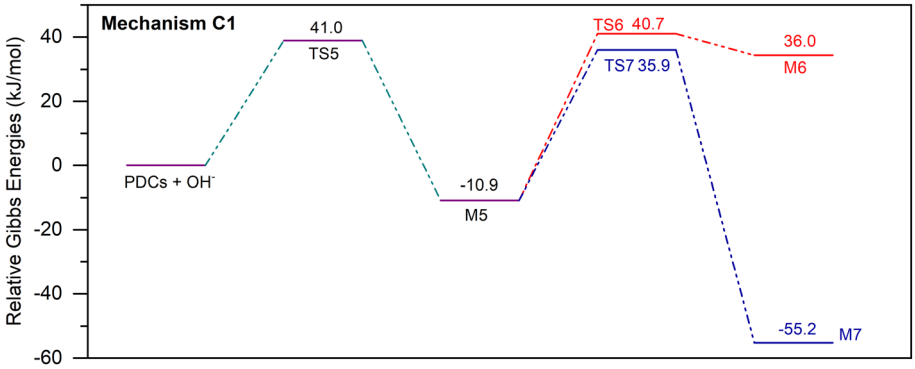

Fig. 12 Potential energy level diagram for ⁻OH attack on C1 in PDC-s. Energies represent relative Gibbs free energies in kJ mol^{-1} at 298 K and 1 atm (ZPE corrections are included).

very distinctive for H abstraction and is equal to 1163i cm^{-1}. The activation barrier for this reaction is relatively low, 49.0 kJ mol^{-1}, as shown in Fig. 13. But the products of this reaction, intermediate M8, and water, lie 65.7 kJ mol^{-1} above the reactant pair. This is mostly due to the unstable nature of M8 caused by replacing an H with a full negative charge on an electronic rich aromatic ring. The importance of this reaction, however, lies in the formation of a very reactive intermediate that can be quickly hydrolyzed to other oxygenated species.

The calculations above were performed at 298 K in aqueous media. However, the experimental conditions were performed at higher temperatures. To understand what such a difference can make, we recomputed the energies of the C1 mechanism at 150, 200, and 250 °C (423, 473, and 523 K). This was done by performing frequency jobs on the optimized species involved in this mechanism at different temperatures, followed by recalculating the activation barriers based on the new thermal corrections. We chose this mechanism over others because it is the most favorable one. The results of this thermal investigation are shown in Fig. 14.

The standard entropy of activation of this reaction is notably negative, −0.16 kJ mol^{-1} K^{-1}. This is due to the decrease in translation entropy associated with combining two reactant species, PDC-s and OH$^-$, into one single transition state. The enthalpy of activation, $\Delta H^{\ddagger}$ is slightly negative, −9.4 kJ mol^{-1}. The changes in $\Delta S^{\ddagger}$ and $\Delta H^{\ddagger}$ over the temperature range of 25–250 °C are not significant as the temperature dependence of these parameters is small within this range. However, the change in $\Delta G^{\ddagger}$ is notable. There is a steady increase in its value as temperature increases. This is because $\Delta G^{\ddagger}$ is a function of both $\Delta S^{\ddagger}$ and $\Delta H^{\ddagger}$ according to the fundamental equation ($\Delta G = \Delta H - T\Delta S$). Since both $\Delta H^{\ddagger}$ and $\Delta S^{\ddagger}$ are negative, with $\Delta S^{\ddagger}$ being highly negative, an increase in T causes the $-T\Delta S$ to become more positive and this leads to an increase in the magnitude of positive $\Delta G^{\ddagger}$. This infer that ⁻OH attacks on the model molecule are not highly favorable at high temperatures.

The activation barriers obtained from these theoretical calculations are in concert with experimental values obtained in the oxycracking of PDC. As Table 2 lists, the E_a values vary

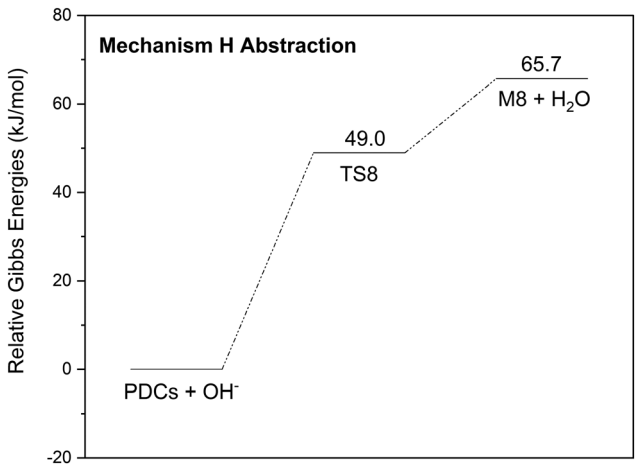

Fig. 13 Potential energy level diagram for H abstraction by ⁻OH in PDC-s. Energies represent relative Gibbs free energies in kJ mol^{-1} at 298 K and 1 atm (ZPE corrections are included).

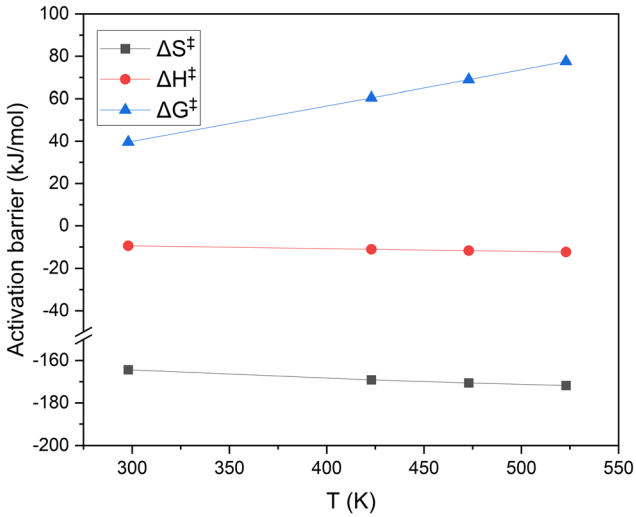

Fig. 14 Changes in the activation barriers $\Delta S^{\ddagger}$, $\Delta H^{\ddagger}$, and $\Delta G^{\ddagger}$ for the C1 mechanism as a function of temperature. The units of $\Delta S^{\ddagger}$ are J mol^{-1} K^{-1}.

between 34 and 66 kJ mol^{-1}, which lies within the range of the theoretical $\Delta G^{\ddagger}$ values. More importantly, the first experimental E_{a1} (42.2 kJ mol^{-1}) agrees very well with that of the C1 mechanism; the most favorable one. This concludes that our theoretical approach was successful in constructing a reaction mechanism for PDC oxycracking.

Conclusion

The thermo-oxidative conversion of residual feedstock model, PDC, has been investigated both experimentally and theoretically as an essential step in understanding its sustainable conversion into valuable products. Three temperatures (150, 200, and 230 °C) and four reaction times (0.5, 1, 1.5, and 2 h) were tested to observe their effects on the oxycracking of PDC under alkaline conditions. Both the starting material and the products were characterized using GC-MS, FTIR, TOC, and elemental analysis. A carbon balance based on the TOC measurements, and the outcomes of the characterizations, were fed into a triangular lumped kinetics model to describe the reaction kinetics of the oxycracking. Along with the experimental work, DFT calculations were performed to explore the thermal oxidation mechanism of PDC. The experimental values of the activation energies agreed with the $\Delta G^{\ddagger}$ values obtained through the DFT calculations. We found that $^{-}$OH plays an important role in initiating the oxycracking reaction of PDC. The most favorable route was found to be the attack of $^{-}$OH attack on the C1 site in PDC, resulting in stable intermediates rich with oxygenated functional groups. Both experimental and theoretical studies showed that the route for full oxidation to CO_2 and water is unfavorable at the range of temperatures and reaction times studied. This is a clear indication that the thermal-oxidation of PDC can be employed as an alternative and sustainable technique for the utilization of residual feedstock to produce value-added products.

Conflicts of interest

There are no conflicts to declare.

Acknowledgements

The authors are grateful to the Natural Sciences and Engineering Research Council of Canada (NSERC) and Alberta Innovates for the financial support through the NSERC Alliance-CASBE program. The authors are also thankful to the Digital Research Alliance of Canada (WestGrid) for supporting this research. I. Badran is thankful to the Department of Chemistry and the Faculty of Sciences at An-Najah National University for their support.

References

1 Global Energy Review: CO2 Emissions in 2020 – Analysis - IEA, https://www.iea.org/articles/global-energy-review-co2-emissions-in-2020 (accessed October 29, 2021).

2 A. D. Manasrah and N. N. Nassar, Oxy-cracking technique for producing non-combustion products from residual feedstocks and cleaning up wastewater, *Appl. Energy*, 2020, **280**, 115890, DOI: 10.1016/J.APENERGY.2020.115890.

3 A. D. Manasrah, N. N. Nassar and L. C. Ortega, Conversion of petroleum coke into valuable products using oxy-cracking technique, *Fuel*, 2018, **215**, 865–878, DOI: 10.1016/j.fuel.2017.11.103.

4 J. J. Adams, Asphaltene adsorption, a literature review, *Energy Fuels*, 2014, **28**, 2831–2856, DOI: 10.1021/EF500282P/ASSET/IMAGES/LARGE/EF-2014-00282P_0004.JPEG.

5 A. D. Manasrah, A. El-Qanni, I. Badran, A. Lante, C. Ortega and M. Josefina Perez-Zurita, *et al.*, Experimental and theoretical studies on oxy-cracking of Quinolin-65 as a model molecule for residual feedstocks †, *React. Chem. Eng.*, 2017, **2**, 703, DOI: 10.1039/c7re00048k.

6 M. Ashtari, L. Carbognani and P. Pereira-Almao, Asphaltenes Aqueous Conversion to Humic and Fulvic Analogs via Oxy-Cracking, *Energy Fuels*, 2016, **30**, 5470–5482, DOI: 10.1021/ACS.ENERGYFUELS.6B00613.

7 F. López-Linares, L. Carbognani, M. F. González, C. Sosa-Stull, M. Figueras and P. Pereira-Almao, Quinolin-65 and violanthrone-79 as model molecules for the kinetics of the adsorption of C7 Athabasca asphaltene on macroporous solid surfaces, *Energy Fuels*, 2006, **20**, 2748–2750, DOI: 10.1021/EF060354X/ASSET/IMAGES/LARGE/EF060354XF00003.JPEG.

8 M. F. González, C. S. Stull, F. López-Linares and P. Pereira-Almao, Comparing Asphaltene Adsorption with Model Heavy Molecules over Macroporous Solid Surfaces, *Energy Fuels*, 2007, **21**(1), 234–241, DOI: 10.1021/EF060196.

9 C. Chen, Y. Diao, Y. Lu, S. Chen and L. Tian, Complete Reaction Mechanisms of Mercury Binding on Petroleum Coke and Brominated Petroleum Coke, *Energy Fuels*, 2019, **33**, 5488–5497, DOI: 10.1021/ACS.ENERGYFUELS.9B00768/ASSET/IMAGES/LARGE/EF-2019-00768C_0010.JPEG.

10 A. Torres, J. Amaya Suárez, E. R. Remesal, A. M. Márquez, J. Fernández Sanz and C. Rincón Cañibano, Adsorption of Prototypical Asphaltenes on Silica: First-Principles DFT Simulations Including Dispersion Corrections, *J. Phys. Chem. B*, 2018, **122**, 618–624, DOI: 10.1021/ACS.JPCB.7B05188/ASSET/IMAGES/LARGE/JP-2017-05188S_0007.JPEG.

11 A. Peraza, M. Sánchez and F. Ruette, Modeling Free-Radical Reactions, Produced by Hydrocarbon Cracking, with Asphaltenes, *Energy Fuels*, 2010, **24**, 3990–3997, DOI: 10.1021/EF1003057.

12 O. C. Mullins, The modified yen model, *Energy Fuels*, 2010, **24**, 2179–2207, DOI: 10.1021/EF900975E/ASSET/IMAGES/LARGE/EF-2009-00975E_0025.JPEG.

13 J. P. Dickie and T. F. Yen, Macrostructures of the Asphaltic Fractions by Various Instrumental Methods, *Anal. Chem.*, 1967, **39**, 1847–1852, DOI: 10.1021/AC50157A057/ASSET/AC50157A057.FP.PNG_V03.

14 N. M. Rodriguez, H. Marsh, E. A. Heintz, R. D. Sherwood and R. T. K. Baker, Oxidation studies of various petroleum

cokes, *Carbon*, 1987, **25**, 629–635, DOI: 10.1016/0008-6223(87)90215-6.

15 M. Legin-Kolar and D. Ugarković, Petroleum coke structure: Influence of feedstock composition, *Carbon*, 1993, **31**, 383–390, DOI: 10.1016/0008-6223(93)90043-A.

16 K. Akbarzadeh, H. Alboudwarej, W. Y. Svrcek and H. W. Yarranton, A generalized regular solution model for asphaltene precipitation from n-alkane diluted heavy oils and bitumens, *Fluid Phase Equilib.*, 2005, **232**, 159–170, DOI: 10.1016/J.FLUID.2005.03.029.

17 R. Q. Lü, J. Lin and Z. Q. Qu, Theoretical study on the interactions between dibenzothiophene/dibenzothiophene sulfone and ionic liquids, *J. Fuel Chem. Technol.*, 2012, **40**, 1444–1453, DOI: 10.1016/S1872-5813(13)60007-9.

18 P. G. Redelius, The structure of asphaltenes in bitumen, *Road Mater. Pavement Des.*, 2011, **7**, 143–162, DOI: 10.1080/14680629.2006.9690062.

19 V. Nemanova, A. Abedini, T. Liliedahl and K. Engvall, Co-gasification of petroleum coke and biomass, *Fuel*, 2014, **117**, 870–875, DOI: 10.1016/j.fuel.2013.09.050.

20 K. Jayaraman and I. Gokalp, Gasification characteristics of petcoke and coal blended petcoke using thermogravimetry and mass spectrometry analysis, *Appl. Therm. Eng.*, 2015, **80**, 10–19, DOI: 10.1016/j.applthermaleng.2015.01.026.

21 I. Badran, A. D. Manasrah and N. N. Nassar, A combined experimental and density functional theory study of metformin oxy-cracking for pharmaceutical wastewater treatment, *RSC Adv.*, 2019, **9**, 13403–13413, DOI: 10.1039/C9RA01641D.

22 M. Coll, J. Frau, F. Muñoz and J. Donoso, Ab Initio Study of the Basic Hydrolysis of the Pyrazolidinone Ring, *J. Phys. Chem. A*, 1998, **102**, 5915–5922, DOI: 10.1021/JP972625Y.

23 J. Kóňa, W. M. F. Fabian and P. Zahradník, Ab initio and DFT studies on the mechanism of ring-opening reactions of 4H-1-benzopyran-4-one with hydroxide ion, *J. Chem. Soc., Perkin Trans. 2*, 2001, **2**, 422–426, DOI: 10.1039/B005731M.

24 R. Sreekanth, K. P. Prasanthkumar, M. M. Sunil Paul, U. K. Aravind and C. T. Aravindakumar, Oxidation reactions of 1- and 2-naphthols: An experimental and theoretical study, *J. Phys. Chem. A*, 2013, **117**, 11261–11270, DOI: 10.1021/JP4081355/SUPPL_FILE/JP4081355_SI_001.PDF.

25 A. Pintar, G. Berčič, M. Besson and P. Gallezot, Catalytic wet-air oxidation of industrial effluents: total mineralization of organics and lumped kinetic modelling, *Appl. Catal., B*, 2004, **47**, 143–152, DOI: 10.1016/J.APCATB.2003.08.005.

26 M. J. Frisch, G. W. Trucks, H. B. Schlegel, G. E. Scuseria, M. A. Robb, J. R. Cheeseman, G. Scalmani, V. Barone, G. A. Petersson and H. L. X. Nakatsuji, *Gaussian 16*.

27 Y. Zhao, D. G. Truhlar, Y. Zhao and D. G. Truhlar, The M06 suite of density functionals for main group thermochemistry, thermochemical kinetics, noncovalent interactions, excited states, and transition elements: two new functionals and systematic testing of four M06-class functionals and 12 other functionals, *Theor. Chem. Acc.*, 2007, **120**, 215–241, DOI: 10.1007/S00214-007-0310-X.

28 R. Peverati and D. G. Truhlar, Quest for a universal density functional: the accuracy of density functionals across a broad spectrum of databases in chemistry and physics, *Philos. Trans. R. Soc., A*, 2014, 372, DOI: 10.1098/RSTA.2012.0476.

29 N. Mardirossian and M. Head-Gordon, Thirty years of density functional theory in computational chemistry: An overview and extensive assessment of 200 density functionals, *Mol. Phys.*, 2017, **115**, 2315–2372, DOI: 10.1080/00268976.2017.1333644/SUPPL_FILE/TMPH_A_1333644_SM5678.ZIP.

30 A. P. Scott and L. Radom, Harmonic Vibrational Frequencies: An Evaluation of Hartree–Fock, Møller–Plesset, Quadratic Configuration Interaction, Density Functional Theory, and Semiempirical Scale Factors, *J. Phys. Chem.*, 1996, **100**, 16502–16513, DOI: 10.1021/JP960976R.

31 M. Ashtari, L. C. Ortega, F. Lopez-Linares, A. Eldood and P. Pereira-Almao, New Pathways for Asphaltenes Upgrading Using the Oxy-Cracking Process, *Energy Fuels*, 2016, **30**(6), 4596–4608, DOI: 10.1021/acs.energyfuels.6b00385.

32 M. Ashtari, L. Carbognani and P. Pereira-Almao, Asphaltenes Aqueous Conversion to Humic and Fulvic Analogs via Oxy-Cracking, *Energy Fuels*, 2016, **30**, 5470–5482, DOI: 10.1021/acs.energyfuels.6b00613.

33 Z. M. Cheng, Y. Ding, L. Q. Zhao, P. Q. Yuan and W. K. Yuan, Effects of supercritical water in vacuum residue upgrading, *Energy Fuels*, 2009, **23**, 3178–3183, DOI: 10.1021/ef900132z.

34 R. Wang, L. Lu, D. Zhang, W. Wei, H. Jin and L. Guo, Effects of Alkaline Metals on the Reactivity of the Carbon Structure after Partial Supercritical Water Gasification of Coal, *Energy Fuels*, 2020, **34**, 13916–13923, DOI: 10.1021/ACS.ENERGYFUELS.0C02735.

35 Z. R. Nasyrova, G. P. Kayukova, Y. V. Onishchenko, V. P. Morozov and A. V. Vakhin, Conversion of High-Carbon Domanic Shale in Sub- and Supercritical Waters, *Energy Fuels*, 2019, **34**, 1329–1336, DOI: 10.1021/ACS.ENERGYFUELS.9B03130.

36 X. Su, L. Guo and H. Jin, Mathematical Modeling for Coal Gasification Kinetics in Supercritical Water, *Energy Fuels*, 2016, **30**, 9028–9035, DOI: 10.1021/ACS.ENERGYFUELS.6B01557.

37 A. Kruse and E. Dinjus, Hot compressed water as reaction medium and reactant, Properties and synthesis reactions, *J. Supercrit. Fluids*, 2007, **39**(3), 362–380, DOI: 10.1016/j.supflu.2006.03.016.

38 L. Li, P. Chen and E. F. Gloyna, Generalized kinetic model for wet oxidation of organic compounds, *AIChE J.*, 1991, **37**, 1687–1697, DOI: 10.1002/AIC.690371112/FORMAT/PDF.

39 The MathWorks Inc., *MATLAB*, 2021.

40 J. P. Lange, R. J. Schoonebeek, P. Mercera and F. W. van Breukelen, Oxycracking of hydrocarbons: chemistry, technology and economic potential, *Appl. Catal., A*, 2005, **283**, 243–253, DOI: 10.1016/J.APCATA.2005.01.011.

41 S. T. Kolaczkowski, F. J. Beltran, D. B. McLurgh and F. J. Rivas, Wet Air Oxidation of Phenol: Factors that May Influence Global Kinetics, *Process Saf. Environ. Prot.*, 1997, **75**, 257–265, DOI: 10.1205/095758297529138.

42 D. A. Patterson, I. S. Metcalfe, F. Xiong and A. G. Livingston, Wet Air Oxidation of Linear Alkylbenzene Sulfonate 2. Effect of pH, *Ind. Eng. Chem. Res.*, 2001, **40**, 5517–5525, DOI: **10.1021/IE010294C**.

43 M. Ashtari, L. Carbognani Ortega, F. Lopez-Linares, A. Eldood and P. Pereira-Almao, New Pathways for Asphaltenes Upgrading Using the Oxy-Cracking Process, *Energy Fuels*, 2016, **30**, 4596–4608, DOI: **10.1021/ACS.ENERGYFUELS.6B00385/SUPPL_FILE/EF6B00385_SI_001.PDF**.

44 A. Tinti, V. Tugnoli, S. Bonora and O. Francioso, Recent applications of vibrational mid-Infrared (IR) spectroscopy for studying soil components: a review, *Journal of Central European Agriculture*, 2015, **16**(1), 1–11, DOI: **10.5513/JCEA01/16.1.1535**.

45 S. F. Sim, L. Seng, N. C. Wong, J. Asing, B. M. N. M. Faizal and A. Satirawaty Bt Mohd Pauzan, Characterization of the coal derived humic acids from Mukah, Sarawak as soil conditioner, *J. Braz. Chem. Soc.*, 2006, **17**(3), 582–587, DOI: **10.1590/s0103-50532006000300023**.

46 L. Yanhong, Z. Yuanqin, Z. Changyu, L. Guangbing and Z. Dengfeng, Method for improving humic acid yield by thermal oxidation of lignite, CN110183682A, 2019.

47 G. Cheng, Z. Niu, C. Zhang, X. Zhang and X. Li, Extraction of humic acid from lignite by KOH-hydrothermal method, *Appl. Sci.*, 2019, 9, DOI: **10.3390/app9071356**.

48 J. Asing, N. C. Wong and S. Lau, Optimization of extraction method and characterization of humic acid derived from coals and composts, *Journal of Tropical Agriculture and Food Science*, 2009, **37**(2), 211–223.

49 R. M. Smith, *Understanding mass spectra: a basic approach*, John Wiley & Sons, 2004.

50 J. R. Pliego, Basic hydrolysis of formamide in aqueous solution: a reliable theoretical calculation of the activation free energy using the cluster-continuum model, *Chem. Phys.*, 2004, **306**, 273–280, DOI: **10.1016/J.CHEMPHYS.2004.07.041**.

51 Y. Jin, Y. Zhu and M. Tang, Theoretical analysis on alkaline hydrolysis mechanisms of N-(2-methoxyphenyl) benzamide, *Comput. Theor. Chem.*, 2011, **2–3**, 268–272, DOI: **10.1016/J.COMPTC.2010.10.036**.

